Optogenetic investigation of cardiac arrhythmia mechanisms

Feola, I.

Chapter 5

OPTOGENETIC MANIPULATION OF ANATOMICAL REENTRY BY LIGHT-GUIDED GENERATION OF A REVERSIBLE LOCAL CONDUCTION BLOCK

Masaya Watanabe*, MD, PhD; Iolanda Feola*, MSc;
Rupamanjari Majumder, PhD; Wanchana Jangsangthong, PhD;
Alexander S. Teplenin, MSc; Dirk L. Ypey, PhD;
Martin J. Schalij, MD, PhD; Katja Zeppenfeld, MD, PhD;
Antoine A. F. de Vries, PhD; Daniël A. Pijnappels, PhD

Laboratory of Experimental Cardiology, Department of Cardiology, Heart Lung Center Leiden; Leiden University Medical Center, the Netherlands.
*equal contribution

Cardiovasc Res 2017; 113:354-366

ABSTRACT

Aims

Anatomical reentry is an important mechanism of ventricular tachycardia, characterized by circular electrical propagation in a fixed pathway. It's current investigative and therapeutic approaches are non-biological, rather unspecific (drugs), traumatizing (electrical shocks) or irreversible (ablation). Optogenetics is a new biological technique that allows reversible modulation of electrical function with unmatched spatiotemporal precision using light-gated ion channels. We therefore investigated optogenetic manipulation of anatomical reentry in ventricular cardiac tissue.

Methods and Results

Transverse, 150-µm-thick ventricular slices, obtained from neonatal rat hearts, were genetically modified with lentiviral vectors encoding Ca^{2+}-translocating channelrhodopsin (CatCh), a light-gated depolarizing ion channel, or yellow fluorescent protein (eYFP) as control. Stable anatomical reentry was induced in both experimental groups. Activation of CatCh was precisely controlled by 470-nm patterned illumination, while the effects on anatomical reentry were studied by optical voltage mapping. Regional illumination in the pathway of anatomical reentry resulted in termination of arrhythmic activity only in CatCh-expressing slices by establishing a local and reversible, depolarization-induced conduction block in the illuminated area. Systematic adjustment of the size of the light-exposed area in the reentrant pathway revealed that reentry could be terminated by either wave collision or extinction, depending on the depth (transmurality) of illumination. *In silico* studies implicated source-sink mismatches at the site of subtransmural conduction block as an important factor in reentry termination.

Conclusions

Anatomical reentry in ventricular tissue can be manipulated by optogenetic induction of a local and reversible conduction block in the reentrant pathway, allowing effective reentry termination. These results provide distinctively new mechanistic insight into reentry termination and a novel perspective for cardiac arrhythmia management.

Key Words

Optogenetics, anatomical reentry, tissue culture, optical mapping, computer-based model.

INTRODUCTION

Anatomical reentry represents a common mechanism of heart rhythm disturbances (*e.g.* ventricular tachyarrhythmias) in structurally damaged myocardium.[1-3] Current approaches to investigate, prevent or terminate this reentrant activity rely on (i) global modulation of cardiac electrical function by drug and electrical shock application, or (ii) local modulation of cardiac electrical activity by introducing a permanent conduction block in the pathway of aberrant propagation through local tissue ablation. In general, however, these three approaches are characterized by their relative unspecific, traumatizing and/or irreversible nature, but also by their limited extent to control cardiac electrical function in time and space.[4-6] In the past few years, optogenetics has emerged as a unique approach to modulate biological function by combining forced expression of light-sensitive proteins with light-emitting diode (LED) technology for tailored activation of these proteins.[7, 8] While first introduced in the field of neuroscience, optogenetics is now also proving its potential in cardiac research, especially in cardiac electrophysiological studies. Here, light-gated ion channels are used to modulate cardiac excitability through generation of de- or hyperpolarizing photocurrents in cardiac muscle cells.[9-13] In two recent studies, the depolarizing optogenetic tool, ChR2(H143R), was used to terminate ventricular arrhythmias in whole murine hearts. These studies, however, address a different research question with another optogenetic tool than ours and come with rather descriptive insight regarding the underlying anti-arrhythmic mechanisms. In the present study we make use of the controllability that in situ models offer to create a model of rat ventricular tachyarrhythmias in which these disturbances are solely based on predefined anatomical reentry. This allowed us to conduct more systematic and detailed studies into the underlying anti-arrhythmic mechanisms of optogenetic interventions. They relied on computer simulations to suggest that Na^+ channel inactivation based on ChR2-dependent depolarization may be involved in the underlying anti-arrhythmic mechanism. In contrast to other, more conventional approaches, optogenetic control of the electrophysiological properties of cardiomyocytes does allow highly specific and fully reversible modulation of cardiac electrical function with unmatched precision. This is especially true if the light-gated ion channels are activated by programmed patterned illumination, as this will allow superb control of cardiac electrical function in space.[14-17] Given the unique research possibilities offered by optogenetics in combination with patterned illumination and its unexplored effects on anatomical reentrant tachyarrhythmias, we were now interested to determine whether and how optogenetic control of electrical function in the pathway of anatomical reentry could be used to manipulate and terminate anatomical reentrant activity in ventricular cardiac tissue. Cultured rat transverse myocardial tissue slices were used to create a standardized and robust *in situ* model of anatomical reentry, in which the L123C mutant of channelrhodopsin-2 (ChR2) from *Chlamydomonas reinhardtii*, designated Ca^{2+}-translocating channelrhodopsin (CatCh), was expressed from a lentiviral vector (LV) and subsequently activated by patterned illumination with 470 nm light. CatCh is more rapidly activated, produces a stronger steady-state current and is approximately 70-fold more sensitive to light stimulation than wild-type ChR2.[18] This distinctive biological approach allowed us

to generate a light-guided, depolarization-induced local conduction block, the presence of which could be tightly controlled in time and space, in any desired area of the tissue slices. This study is the first to demonstrate that such optogenetic manipulation in the pathway of anatomical reentry could terminate the arrhythmic activity, thereby revealing a new mechanism of anatomical reentry termination based on precise, transient and non-destructive modulation of electrical function, *i.e.* without drugs, electrical shocks or tissue damage.

MATERIALS AND METHODS

A detailed description of materials and methods can be found in the Supplementary Material online. All animal experiments were approved by the Animal Experiments Committee of Leiden University Medical Center (LUMC) and done in accordance with the Guide for Care and Use of Laboratory Animals as stated by the US National Institutes of Health.

Preparation of transverse rat ventricular tissue slices

After perfusion of the hearts of neonatal Wistar rats with oxygenated phosphate-buffered saline (PBS) containing 10 IU/ml heparin, transverse ventricular tissue slices 150-µm thick were obtained using a vibratome (VT1200S, Leica Microsystems, Rijswijk, the Netherlands). The slices were kept under culture conditions at 37°C in humidified 95% air-5% CO_2 for 4 days.

Lentiviral gene transfer

The cardiac tissue slices were genetically modified at the day of production by adding concentrated viral vector suspension directly on top of the slices and into the medium under the semi-porous membrane in the presence of 10 µg/ml diethylaminoethyl-dextran (Carl Roth, Karsruhe, Germany).

Patch clamp

Patch clamp recordings were performed using an inverted microscope Zeiss Axiovert 35 (Carl Zeiss, Oberkochen, Germany) with an integrated LED-based 470-nm light illumination device (M470L3 collimated LED; Munich, Germany). Patch clamp equipment consisted of a MultiClamp 700B amplifier and a Digidata 1440A A/D converter controlled by commercially available MultiClamp 700B Commander and Clampex v10.3 software (Molecular Devices, Sunnyvale, CA). Perforated patch clamp recordings in current- and voltage-mode were obtained from single neonatal rat ventricular cardiomyocytes expressing CatCh (CatCh-NRVCs)

Integrated system for optical mapping and patterned illumination

The optical mapping system was engineered by integration of a patterned illumination device, the Polygon400 (Mightex Systems, Toronto, ON) to allow recording of electrical activation with the voltage-sensitive dye Di-4-ANEPPS (Life Technologies Europe, Bleiswijk, the Netherlands) and patterned illumination with blue light (470 nm), (Figure S1C). Slices were stimulated either electrically with an epoxy-coated unipolar platinum electrode (FHC, Bowdoin, ME) using

2-ms rectangular pulses of 1.5 V or optically with 10-ms/470-nm light pulses (0.68 mW/mm^2), coming from the Polygon400. Reentry was induced by electrical pacing using S1-S2 electrical protocol. After confirmation of the presence of reentrant conduction, slices were exposed to 470-nm LED light for 500 ms using the patterned illumination device.

Numerical Methods

The NRVCs were modeled according to the formulation of Korhonen *et al*,[19] with adaptations by Hou *et al*[20] The complex intracellular Ca^{2+} diffusion between the sarcolemma and the perinuclear sarcoplasmic reticulum was replaced by a simple Ca^{2+}-handling process adopted from tenTusscher *et al*[21] Cardiac myofibroblasts were modeled according to the passive formulation of MacCannell *et al*,[22] whereas the empirically derived model of ChR2 (current-enhanced mutant H134R) by Williams *et al*[23] was used together with the parameter set established by Boyle *et al*[24] to implement optogenetics. Eight confluent monolayer stripes (12.75 × 2.8 mm) were constructed as arrays of 1145 cell sites with 17% myofibroblasts. Each stripe was electrically paced from one side, at a CL of 500 ms, with a 2-ms current stimulus of 100 pA . Wave propagation was then studied in the stripes in the presence of virtual irradiation over a rectangular area 600 μm × 25% or 75% of the transmural width (2.8 mm).

Statistical analysis

Data were expressed as mean ± standard deviation. Comparison between 2 groups was performed with Student's t-test for continuous variables and with the X^2 test for categorical variables. When data were analyzed across more than 2 variables, analysis of variance (ANOVA) was used. Parameters before and after reentry termination were compared using paired t-tests. To take into account both the number of slices and the number of animals, mixed model of analysis was also performed, when applicable. Differences were considered statistically significant at $P<0.05$. Statistical analyses were performed with SPSS11.0 for Windows (SPSS, Chicago, IL) and JMP pro 12 for Windows (SAS, Cary, NC).

RESULTS

Electrophysiological effects of CatCh activation

To study the electrophysiological effects of light-mediated CatCh activation, perforated patch clamp experiments were performed on single CatCh-NRVCs. In a previous study from our research group, a 500-ms/470-nm light pulse sufficed to characterize the kinetics of the CatCh-generated photocurrent in atrial cardiomyocytes.[25] For this reason, CatCh-NRVCs were exposed to 500-ms blue light pulses in combination with different light intensities to determine the minimum light intensity required to evoke an action potential (AP) and generate a stable voltage plateau during the repolarization phase, *i.e.* prolonged depolarization (Figure S2A). Plotting the mean voltage shift at the end of the 500-ms light pulse against light intensity (n=5 for each condition; Figure S2B) revealed that the prolonged depolarization was characterized by voltage shifts from resting potential of 17.7±20.8 mV for a light intensity of 0.03 mW/mm^2 to

65.5±4.2 mV for a light intensity of 2.6 mW/mm^2. Since the maximum voltage shift was already reached at light intensity of 0.65 mW/mm^2, this light intensity was applied for 5, 50, 500 or 5000 ms to stimulate CatCh-NRVCs. As shown in Figure 1B, the duration of the plateau phase was determined by the duration of the light pulses. Voltage-clamp recordings demonstrated that illumination with 470-nm light for 500 ms induced typical CatCh inward currents at negative holding potential of -40 mV (n=7) (Figure 1C). Peak (I_{pk}) and steady-state (I_{ss}) CatCh photocurrents were 37.9±9.0 and 25.5±5.9 pA/pF, respectively. Moreover, CatCh partially desensitized with a time constant (t_{des}) of 447.6±109.1 ms as determined by a single-exponential fit to the current decay after the peak (Figure 1C). The channel closing time constant (t_{off}), determined by a two-component exponential fit to the current decay after illumination (Figure 1C), was 103.1±26.7 and 965.9±304.8 ms for fast and slow components, respectively. These findings confirmed the presence of a CatCh-generated photocurrent and proof its potential to keep CatCh-NRVCs in a depolarized state.

Histological characterization of cardiac tissue slices

Micrographic analyses of transverse neonatal rat ventricular tissue slices revealed that after transduction with the CatCh-encoding LV (CatCh↑ group) or the enhanced yellow fluorescent protein (eYFP)-encoding control vector (eYFP↑ group) (for vector maps,Figure 1A) and 4 days of culture, these slices maintained their gross anatomy, including the presence of both the left and right ventricular lumen (Figure 1D, left panel). In addition, the tissue slices showed the abundant presence of nuclei in a homogenous distribution pattern and, importantly, global transgene expression (Figure 1D, middle and right panel, respectively). Due to the use of the striated muscle-specific MHCK7 promoter, transgene expression was only observed in α-actinin$^+$ cells (*i.e.*, cardiomyocytes). Of the cardiomyocytes, 63±13% expressed CatCh, which was mainly localized at the sarcolemma (Figure 1E and F). Immunohistological analysis for sarcomeric α-actinin showed a typical cross-striated expression pattern in both groups, indicating preservation of sarcomeric organization (Figure S3A). Moreover, the gap junction protein connexin43 (Cx43) and the fibroblast marker collagen type 1 (Col1) showed the characteristic staining patterns for these proteins in both the CatCh↑ and eYFP↑ group (Figure S3B and S3C). Immunostaining for cleaved caspase-3 demonstrated lack of apoptotic activity in the large majority of cells (Figure S3D). Cell viability was also investigated by Mitotracker staining for active mitochondria, which showed intense and uniform labeling (Figure S3E).

Electrophysiological characterization of cardiac tissue slices

To investigate their basic electrophysiological properties, such as action potential duration at 80% repolarization (APD_{80}) and conduction velocity (CV), slices were loaded with the voltage-sensitive dye Di-4-ANEPPS and subjected to high-resolution optical mapping while being electrically stimulated at 1-9 Hz. In this study, optical voltage mapping was performed with Di-4-ANEPPS mapping instead of Di-4-ANBDQBS because of a better signal-to-noise ratio and a lack of significant adverse electrophysiological effects (Figure S4). Neither the eYFP↑ slices

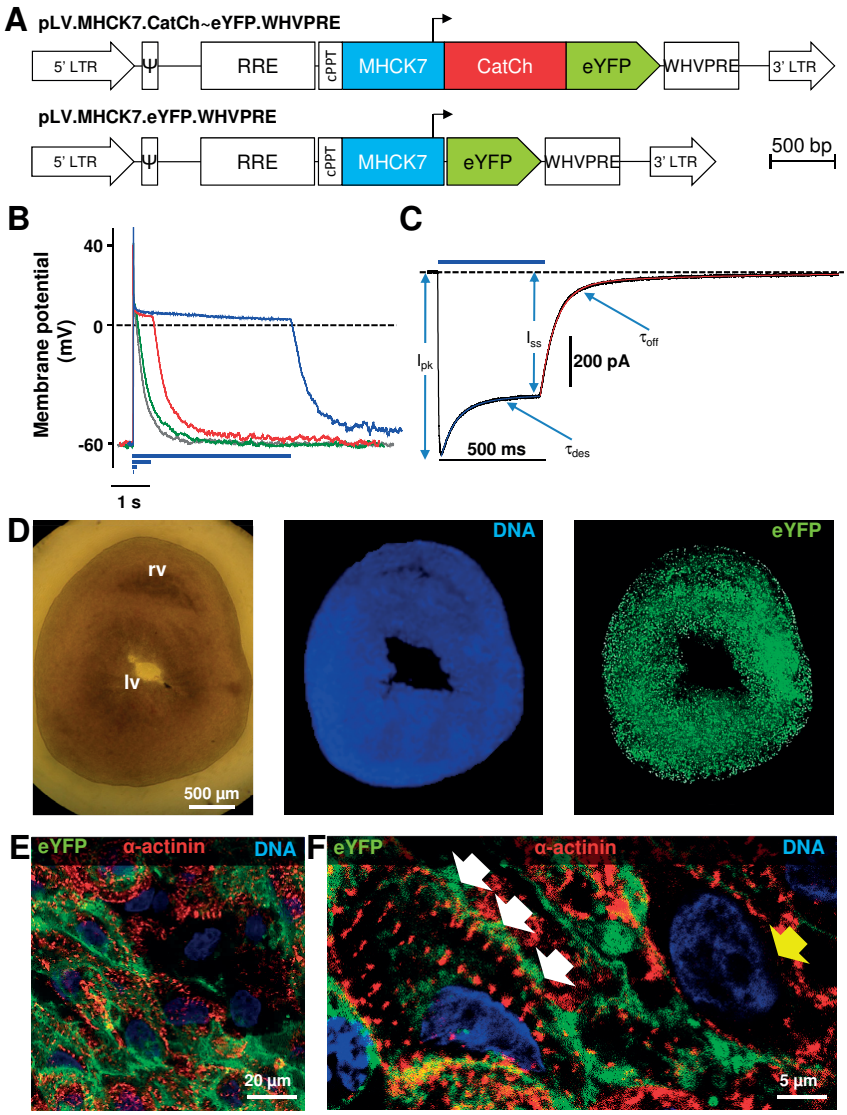

Figure 1. Characterization of CatCh-photocurrent. A, Structure of LV shuttle plasmids pLV.MHCK7.CatCh~eYFP.WHVPRE (for generating LV.CatCh~eYFP↑) and pLV.MHCK7.eYFP.WHVPRE (to produce LV.eYFP↑). 5' LTR: chimeric 5' long terminal repeat containing enhancer and promoter elements of the human cytomegalovirus immediate-early gene and the human immunodeficiency virus type 1 (HIV1) R and U5 regions. Ψ: HIV1 packaging signal. RRE: HIV1 Rev-responsive element. cPPT: HIV1 central polypurine tract and termination site. MHCK7: chimeric striated muscle-specific promoter. CatCh: coding sequence of mutant of the light-gated ion channel ChR2. eYFP: Aequorea victoria enhanced yellow fluorescent protein-coding sequence. WHVPRE: woodchuck hepatitis virus post-transcriptional regulatory element. 3′ LTR: wild-type 3′ HIV1 LTR. B, Representative membrane potential recordings of CatCh-NRVCs upon blue light stimulation at 0.65 mW/mm^2 for 5, 50, 500 and 5000 ms (n=5). C, Typical inward photocurrent evoked at a holding potential of -40 mV by exposure of a CatCh-NRVC to a 500-ms blue light pulse at 0.65 mW/mm^2 irradiance. D, Microscopic images of a slice after transduction with LV.CatCh~eYFP↑ and 4 days

of culture. Left panel, brightfield image, middle panel, fluoromicrograph showing Hoechst 33342-stained nuclei, right panel, fluorescent micrograph showing CatCh~eYFP expression. (E and F) High magnification images showing CatCh expression at the sarcolemma of α-actinin^{+} cells (*i.e.*, cardiomyocytes; white arrows). As transgene expression was driven by the striated muscle-specific MHCK7 promoter, CatCh was not expressed in α-actinin- cells (yellow arrow) (n=3 slices, 3 rats). lv, left ventricle. rv, right ventricle. bp, base pairs.

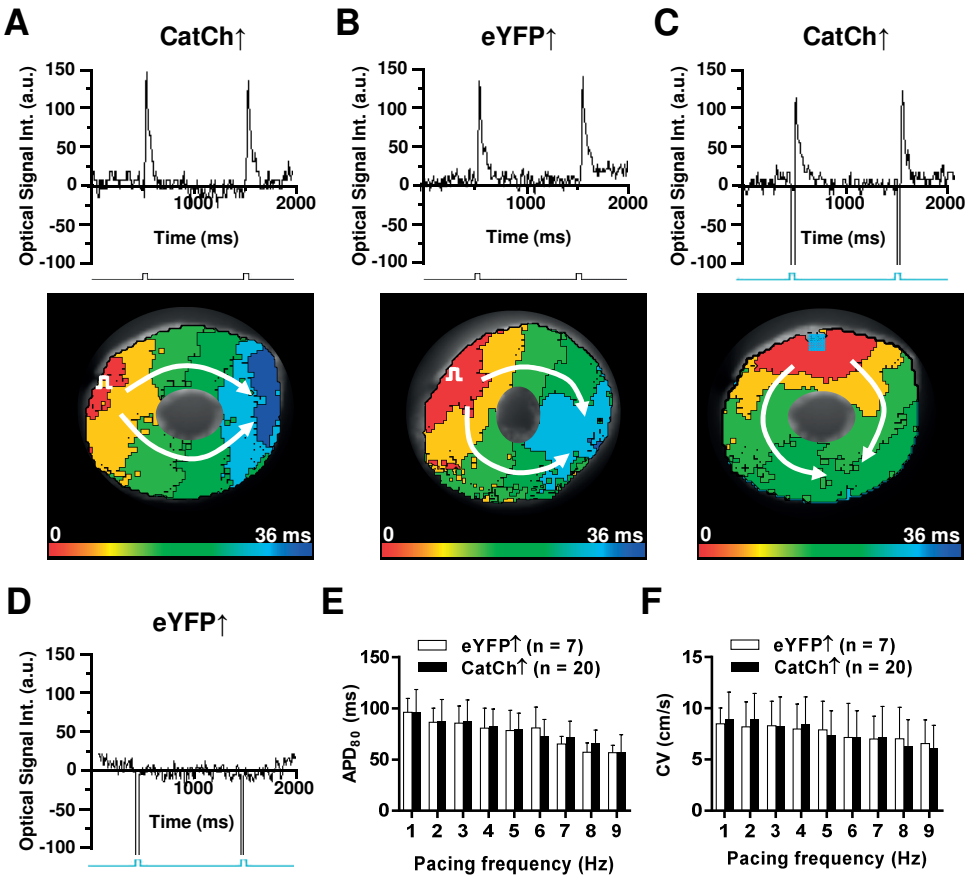

Figure 2. Electrophysiological characteristics of cultured ventricular slices. A and B, Representative optical traces (top) and activation maps (bottom) of CatCh↑ (A) and eYFP↑ (B) slice during 1-Hz electrical stimulation. C, Representative optical trace (top) and activation map (bottom) of CatCh↑ slice following local 10-ms exposure to blue light of 470 nm. D, Typical example of the optical trace resulting from local 10-ms exposure of an eYFP↑ slice to blue light of 470 nm. E and F, CatCh↑ (n=20 slices, 9 rats) and eYFP↑ (n=7 slices, 4 rats) slices display similar APD_{80} (E) and CV (F) values during electrical stimulation at different pacing frequencies with higher pacing frequencies resulting in shorter APDs and slower conduction by two-way ANOVA. Of note, random effects model also showed no difference between CatCh↑and eYFP↑ slices.

(n=7) nor the CatCh↑ slices (n=20) showed spontaneous activity. However, electrical point stimulation evoked APs in all slices in both groups and resulted in bidirectional propagation of the electrical wavefront around the left ventricular lumen followed by its annihilation at the collision site (Figure 2A and 2B). At a pacing frequency of 1 Hz, no significant differences were observed in APD_{80} or CV between CatCh↑ and eYFP↑ slices; APD_{80} was 96±13 ms vs 96±22 ms (P=0.43), and CV was 8.9±2.7 vs 8.4±1.6cm/s (P=0.99), respectively. As pacing frequency increased from 1 to 9 Hz, the values of these parameters gradually decreased in a similar fashion for both groups (Figure 2E and 2F). From these data, we concluded that there are no major differences in excitability, gap junctional coupling and restitution properties between the CatCh↑ and eYFP↑ groups. To investigate whether transduction of cardiac tissue slices with CatCh-encoding LV particles resulted in light-gated ion channel activity, these slices were exposed, by patterned illumination, to brief light pulses (10-ms; 470-nm) targeting a 300-μm square area near the tissue border. As anticipated, APs could be readily evoked by 470-nm light exposure of the CatCh↑ slices while optical stimulation of the eYFP↑ slices did not produce APs (Figure 2C and 2D). Consistently, following blue light exposure only the CatCh↑ slices showed contractions. Together these results indicate that transverse ventricular tissue slices can be derived from neonatal rat hearts and kept in culture for at least 4 days without losing the key anatomical properties and the capability to generate and propagate electrical signals. This culture period suffices to optogenetically modify the cardiac tissue slices with LVs encoding a light-gated depolarizing ion channel, thereby allowing optical control of excitability in these slices.

Induction and characterization of anatomical reentry

In order to test the effects of optogenetic manipulation on anatomical reentry, such arrhythmic activity was induced in the cardiac tissue slices by dedicated electrical stimulation according to the so-called extra stimulus S1-S2 protocol.[26] The bifurcated wavefront of each S1 stimulus propagated around the left ventricular lumen of the slice and its two parts finally collided at the end of the slice opposite of the pacing electrode (Figure 3A, left activation map). The subsequent S2 stimulus was given at a progressively shorter time interval until unidirectional S2 propagation occurred and reentry was initiated (Figure 3A, middle activation map and right panel of optical records). Typically, reentry was pinned to the left ventricular lumen with activation of the right ventricle following each reentrant cycle (Figure 3A, right activation map). The S1-S2 protocol resulted in sustained reentry in 86% (6 out of 7) and 85% (40 out of 47) of the eYFP↑ and CatCh↑ slices, respectively (P=0.97, Figure 3B). No significant differences were observed in reentry CL (120±42 vs 110±20 ms, P=0.33, Figure 3C), APD_{80} (56±14 vs 57±11 ms, P=0.72, Figure 3D) and CV (3.7±0.8 vs 4.4±1.3 cm/s, P=0.23, Figure 3E) between both groups, which suggests that the optogenetic modification itself did not affect either reentry inducibility or key properties of the resulting tachyarrhythmia.

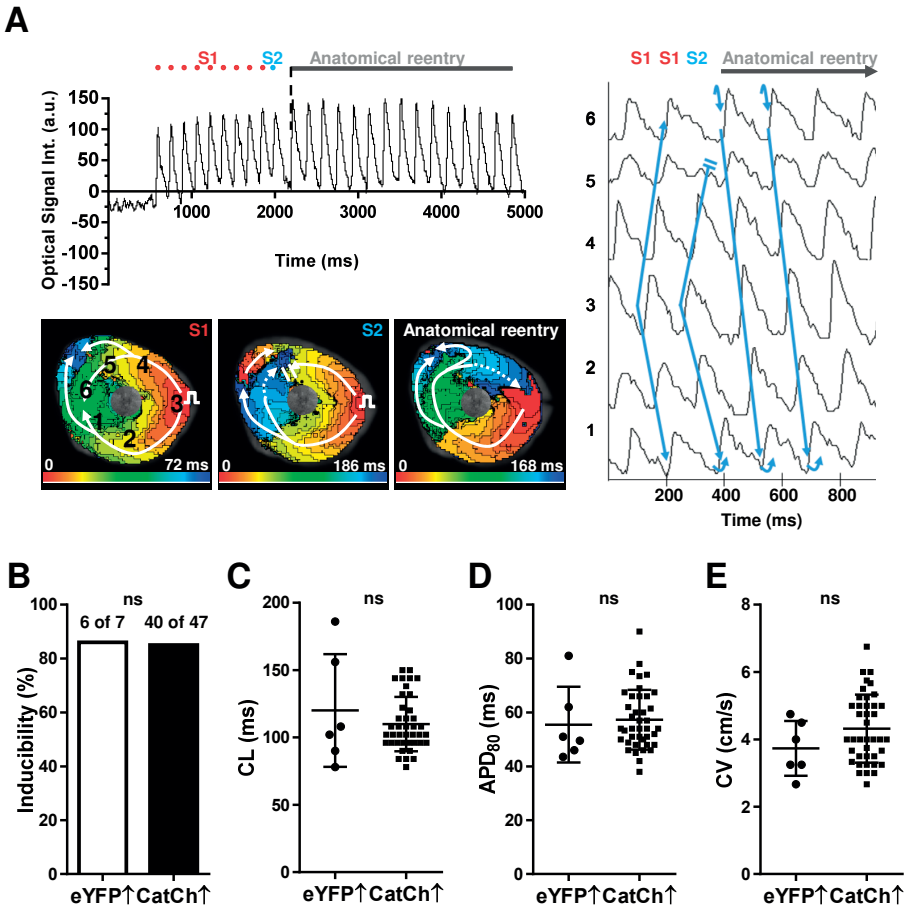

Figure 3. Induction and characterization of anatomical reentry. A, Representative optical trace (left, top) and activation maps (left, bottom) of a CatCh↑ slice subjected to S1-S2 electrical stimulation to induce anatomical reentry. The right panel shows enlarged optical traces derived from positions 1 through 6 in the slice at the moment in which anatomical reentry is established. No significant difference was observed in anatomical reentry inducibility (B) between eYFP↑ (n=7 slices from 4 rats) and CatCh↑ (n=47 slices from 13 rats) by X^2 test, nor in the CL (C), APD_{80} (D) and CV (E) during reentry between groups (6 slices from 4 rats in eYFP↑ and 40 slices from 13 rats in CatCh↑) by both student t-test and random effects models.

Effects of global illumination on anatomical reentry

Before testing the effects of illuminating only a local area in the pathway of aberrant conduction (see below), the effects of global illumination on ongoing anatomical reentry were assessed. After the presence of reentry was confirmed by optical mapping, the entire area of the slices was exposed to 470-nm light for a duration of 500 ms, based on CatCh t_{des} (Figure 4A and 4B). Such global illumination terminated reentry in all CatCh↑ slices (n=23), but none of the eYFP↑ slices (n=6) ($P<0.01$) (Figure 4C).

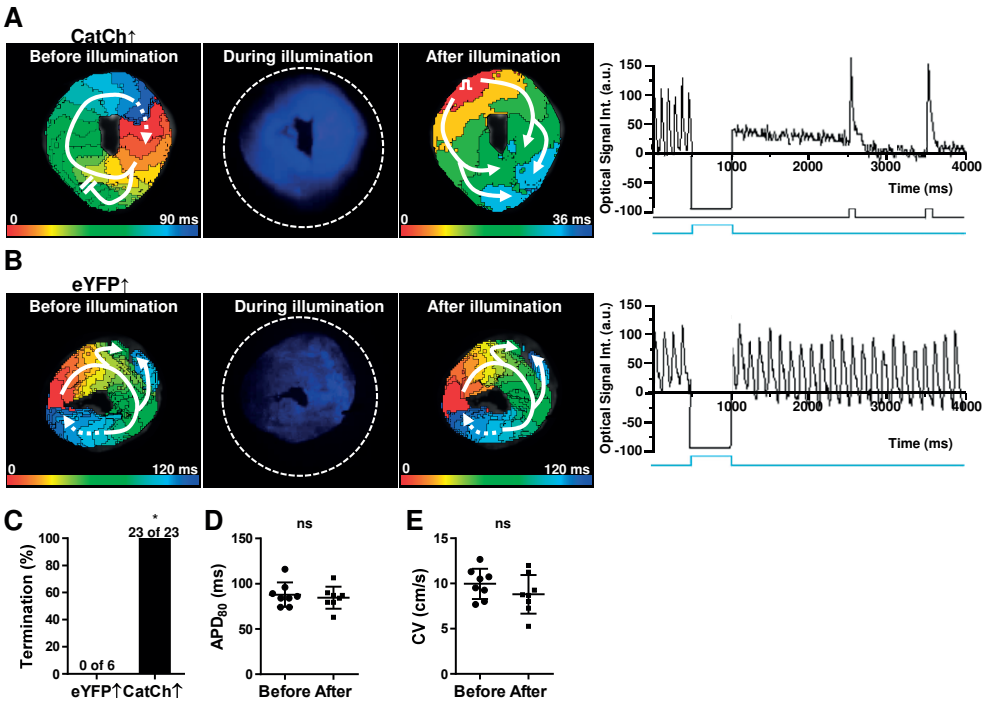

Figure 4. Effects of global illumination on anatomical reentry. A and B, Representative activation maps before and after 500-ms exposure to 470-nm light (left, first and third panels), screen shots taken during the illumination period (left, middle panel) and corresponding optical traces (right) of CatCh↑ and eYFP↑ slices, respectively. CatCh↑ slices showed uniform AP propagation when electrically stimulated at 1 Hz at 1.5 s after illumination (A). Global 470-nm light exposure of eYFP↑ slices did not affect reentrant activity (B). C, Incidence of successful anatomical reentry termination in CatCh↑ (n=23 slices from 8 rats) and eYFP↑ (n=6 slices from 4 rats) slices. Statistical comparison was made using X^2 test. * P<0.001. No differences were observed in APD_{80} (D) and CV (E) during electrical stimulation at 1 Hz of CatCh↑ slices (n=8 slices from 2 rats) before and after reentry termination using both paired t-test and mixed effect model analysis.

To investigate potential aftereffects of the optogenetic intervention on key electrophysiological properties of the cardiac tissue slices, 1-Hz electrical stimuli were given 1.5 s after global illumination of the CatCh↑ slices (n=8) (Figure 4A, right). The APs evoked before and after illumination did not display significant differences in APD_{80} (87±14 vs 84±12 ms, P=0.55) or CV (10.0±1.7 vs 8.8±2.1 cm/s, P=0.13) (Figure 4D and 4E). These results indicate that anatomical reentry in these cardiac slices could be terminated effectively by global transient light-induced activation of CatCh without compromising subsequent normal electrical activation.

Termination of anatomical reentry by local illumination

Next, the effect of programmed regional illumination of the CatCh↑ slices, and therefore local generation of a depolarizing photocurrent, on sustained anatomical reentry was investigated.

First, an area spanning the entire thickness of the myocardium (fully transmural) and 300 or 600 μm in width was illuminated for 500 ms using the patterned illumination device (Figure 5A and 5B). This local activation of CatCh in the pathway of reentrant conduction resulted in 57% (8 out of 14) and 100% (14 out of 14, $P<0.01$) arrhythmia termination, respectively (Figure 5C). In all cases, arrhythmic activity was terminated by collision of the reentrant wave into the area of CatCh activation-induced temporary conduction block. Of note, in the six cases in which reentry was not terminated, the reentrant CL increased during illumination (Figure 5D). Importantly, re-induction of reentry in 4 of the preparations followed by local illumination of 3 other areas divided over the left ventricular wall again resulted in arrhythmia termination, indicating that this was not a local phenomenon. These data show that not only global illumination but also predefined regional illumination of only a small area of the pathway of reentrant conduction leads to termination of anatomical reentry in optogenetically modified cardiac tissue slices. Activation of CatCh by local transmural illumination resulted in acute generation of a regional and temporary conduction block in which the reentrant wavefront collided, thereby interrupting the reentrant pathway and causing termination of the arrhythmia. After having shown the effects on anatomical reentry of a reversible conduction block spanning the full transmural thickness of a cardiac tissue slice, the anti-arrhythmic potential of subtransmural illumination was investigated. We hypothesized that subtransmural illumination would cause local narrowing of the pathway of reentrant wave conduction, thereby creating a so-called isthmus (Figure 6A and 6B).

The width of the illuminated area was fixed at 600 μm, while its transmurality (*i.e.* depth) was gradually increased from ¼, ½, ¾ till 1 (*i.e.* full transmurality) resulting in a systematic narrowing of the isthmus until it was no longer present. As shown in Figure 6C, reentry could be terminated in all 4 situations but the success rate of termination increased from 2 (10%), 5 (24%), 9 (43%) to 21 (100%) out of 21 slices with an increase in transmurality of illumination from ¼, ½, ¾ to 1, respectively.

Analysis of the dynamics of the reentrant wavefront during illumination showed that in cases of failed arrhythmia termination, the wavefront passed through the isthmus, thereby allowing reentry to continue (Figure 6A).

Of note, the CLs of the reentrant circuits that could not be terminated increased during illumination (Figure 6D), indicating that optogenetic manipulation of anatomical reentry could also slow down the ongoing reentrant tachyarrhythmia. In case of termination, however, the wavefront entered the isthmus and faded away (*i.e.* wave extinction), while the remainder of the wavefront collided directly into the light-induced conduction block (Figure 6B). Reentry termination occurred at the site of illumination with the exception of two cases (Figure 6E), in which conduction became slower after passing the illuminated area and eventually stopped, thereby still resulting in arrhythmia termination. Together these results demonstrate that light-guided generation of a local and reversible conduction block, which is only partially obstructing the pathway of reentrant conduction, may result in arrhythmia termination. Whether the temporary isthmus between the ventricular lumen and the area of reversible conduction block allowed conduction of reentrant waves depended on its width. By narrowing

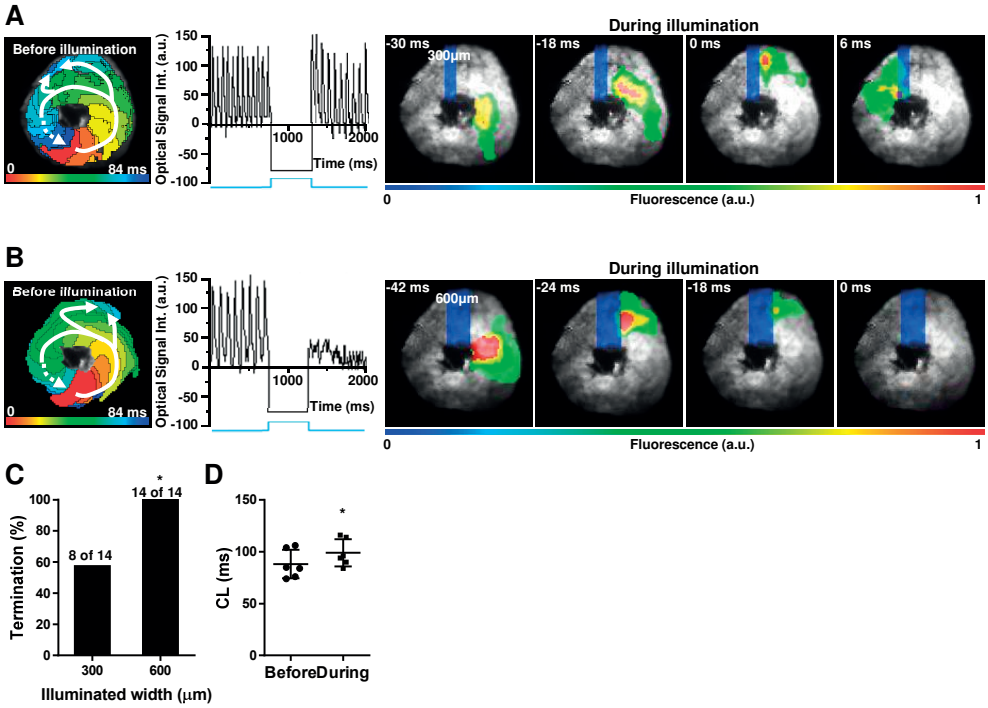

Figure 5. Reentry termination by local transmural illumination of CatCh↑ slices. A and B, Typical activation maps confirming the presence of anatomical reentry before 500-ms exposure to 470-nm light (left), traces showing the optical signal before and after illumination (middle) and wave propagation during light exposure (right four panels). Example of a reentrant activation wavefront passing through a light-exposed transluminal area 300 µm in width (A). Example of successful reentry termination when the width of the light-exposed transluminal area is increased to 600 µm (B). C, The success rate of light-induced anatomical reentry termination depends on the width of the illumination area. Statistical comparison was made using X^2 test. * P<0.01 (n=14 slices from 5 rats). D, Passage of reentrant circuits through the 300-µm wide transmural illuminated area slightly but significantly increased their CL. * P<0.05 using both paired t-test and mixed effect model analysis (n=6 slices from 4 rats).

this isthmus via deeper transmural illumination, reentrant conduction more often faded away causing arrhythmia termination. These findings suggest that a so-called electrical source-sink mismatch at the temporary isthmus could play an important role in the mechanism of reentry termination. In other words, narrowing the isthmus would lead to an increase in source-sink mismatch and thereby raise the chance of AP propagation failure at the isthmus.

In silico studies into the mechanisms underlying block of propagation

To study the role of electrical source-sink relationships in block of AP propagation caused by local subtransmural illumination, computer simulations were performed. If mismatches between source and sink play an important role, their functional modulation (from mismatch to match and vice versa) should change the experimental outcome (from continued propagation

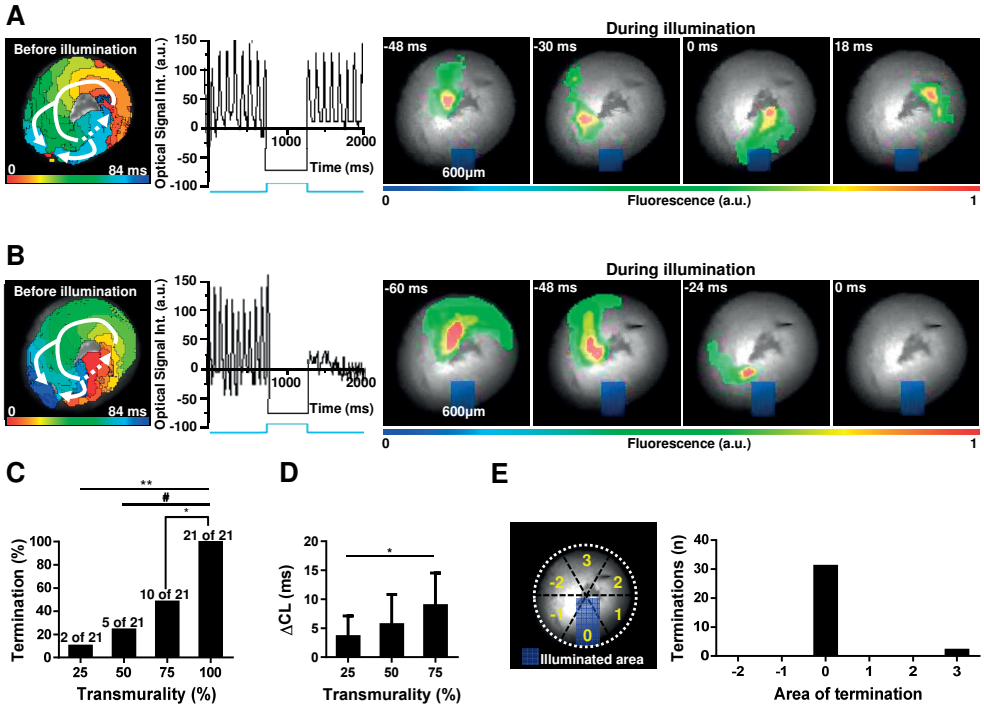

Figure 6. Reentry termination by local subtransmural illumination of CatCh↑ slices. A and B, Representative activation maps confirming the presence of anatomical reentry before 500-ms exposure to 470-nm light (left), traces showing the optical signal before and after illumination (middle) and wave propagation during light exposure (right four panels). Example of unsuccessful reentry termination following illumination of a 600-µm wide area spanning 25% of the total width of the myocardial wall (A). Example of successful reentry termination in a CatCh↑ slice by illumination of a 600-µm wide area spanning 50% of the total width (B). C, The success rate of light-induced anatomical reentry termination shows a positive correlation with the extent of transmurality of the 600-µm wide light-exposed area. * P<0.001 vs 75%, # P<0.001 vs 50%. ** P<0.001 vs 25% using X^2 test (n=21 slices from 10 rats). D, Increases in transmurality of illumination result in larger increases in reentry CL during failed optogenetic arrhythmia termination. * P<0.05 75% vs 25% using one-way ANOVA with post-hoc Bonferroni's test. Similarly, random effects one-way ANOVA showed significant difference (P<0.001). E, Analysis of the incidence of reentry termination in different parts of the slice (equal-sized segments -2, -1, 0, 1, 2, 3) showing that reentry termination rarely occurs outside of the illuminated area (*i.e.* segment 0).

to conduction block and vice versa). For these studies, we created virtual NRVC monolayer strips of 12.75 × 2.8 mm, in which ChR2 was uniformly incorporated into the cardiomyocytes, thereby mimicking the area of interest in the cultured cardiac tissue slices. Left-sided electrical stimulation of the strip resulted in uniform AP propagation towards the other side of the strip (Figure 7A, left panel). Next, the light-sensitive ion channels were activated by *in silico* illumination of a rectangular central area of 600 µm × 25% or 75% of the total strip width (Figure 7A, right panels). After creation of a functional conduction block by illuminating 25% of the total strip width, 37.5% of the strips showed 1:1 propagation of the evoked electrical signal

to the right side of the strip, whereas 62.5% showed 1:2 propagation, thus no complete block (Figure 7B). In contrast, illumination of 75% of the total width resulted in complete block of AP propagation at the site of illumination in all strips and in all cases (Figure 7C). The voltage distribution in the strips around this site confirmed the generation of a functional conduction block through depolarization.

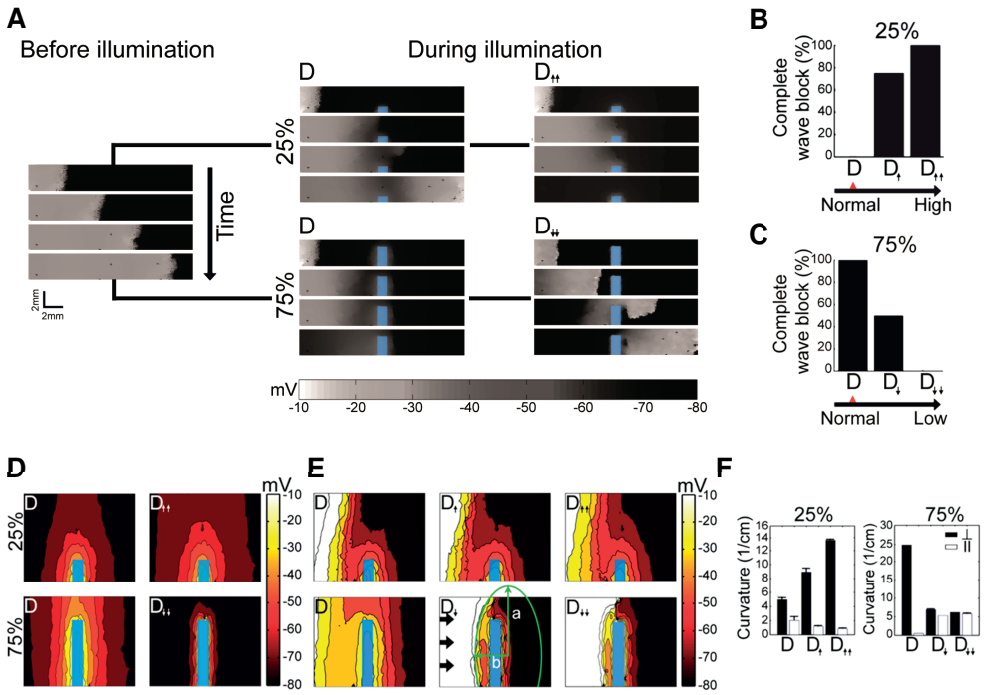

Figure 7. *In silico* study into the mechanism underlying block of AP propagation caused by partial obstruction of the conduction pathway. A, Propagation of APs evoked by electrical stimulation through 2.8-mm wide strips containing ChR2-expressing cardiomyocytes before (left) and during (right) illumination. When 25% of the total strip width (upper right panels) with normal intercellular coupling (D) is illuminated, APs propagate successfully through the isthmus, while propagation is blocked with 2-fold increased intercellular coupling (D↑↑). When 75% of the total strip width (lower right panels) with normal intercellular coupling (D) is illuminated, propagation is blocked following conduction slowing. Decreasing the intercellular coupling 25-fold (D↓↓) enables wave propagation through the isthmus. B and C, Quantification of successful complete blockage of AP propagation at different levels of intercellular coupling and illumination of 25% (B) or 75% (C) of the total strip width. D, Voltage distribution in the depolarization gradients formed around illuminated rectangles covering 25% (upper panels) and 75% (lower panels) of the total strip width with normal (D, left panels) or increased and decreased (D↑↑ and D↓↓, right panels) intercellular coupling in the absence of electrical stimulation. E, Visualization of voltage around the area of illumination at the instant when the wave impinges on the light-exposed area. By increasing the intercellular coupling the wavefront becomes increasingly concave, while decreasing leads to straightening of the wavefront. F, Quantification of longitudinal curvature (||, b/a2) and transverse curvature (⊥, a/b2) of the wavefront impinging on light-exposed rectangles covering 25% (left) or 75% (right) of the total strip width. a, major radius. b, minor radius.

This area was characterized by a gradient of membrane potentials ranging from -20 mV in the center to -30 mV at the border of the illuminated area and to -70 mV in the most distal affected region outside of the illuminated area (Figure 7D, left frames). In areas with potentials ≳ -45 mV, fast Na^+ channels were no longer available for excitation, causing the area of light-induced conduction block to extend well beyond the illuminated region. In addition, conduction slowing was observed in the regions with membrane potentials ranging between -45 mV and -65 mV, and therefore with a limited availability of fast Na^+ channels. Once established, such conduction block and partially depolarized neighboring regions seem to favor failure of AP propagation at the site of illumination. The degree to which depolarization extended into the areas surrounding the illuminated zone was tested in CatCh↑ slices through optical mapping with Di-4-ANBDQBS. The CatCh↑ slices were electrically stimulated at a frequency of 7-9 Hz prior and during illumination of a 600-µm-wide rectangular area of 25 or 75% transmurality. The gradient in depolarization was assessed by comparing the AP amplitude, before and during illumination, in 3 different spots at increasing distance from the targeted area. This comparison supported the results of the *in silico* study by showing that the optical signal amplitude was most strongly reduced (~50%) in the spot closest to the area of illumination (Figure 8).

To investigate whether electrical source-sink relationships are indeed a key factor underlying block of propagation at the site of illumination, and hence reentry termination, this relationship was modulated in a stepwise manner. Intercellular coupling, or gap junctional conductance, is considered to be an important determinant of passive voltage spread.[27] We therefore varied the mathematical coefficient of voltage diffusion (D), which biophysically correlates with gap junctional conductance, to study its effects on AP propagation at the site of conduction block. For strips in which only 25% of the total width was illuminated, a 1.5-fold increase in D (D↑) led to full conduction block in 75% of the strips (Figure 7B), while 12.5% showed 1:2 capture and 12.5% exhibited 1:3 propagation to the right side of the strips. Increasing D 2-fold (D↑↑), resulted in complete failure of propagation at the site of block in all cases (Figure 7B). Such improved gap junctional conductance increased the spatial spread of the depolarization gradients and consequently increased the size of the inexcitable area, further reducing the opportunities for wave propagation (Figure 7E, D↑ and D↑↑). A quantitative analysis of the curvature of the incoming wavefront showed that as conductance increased, the ratio (r) of longitudinal

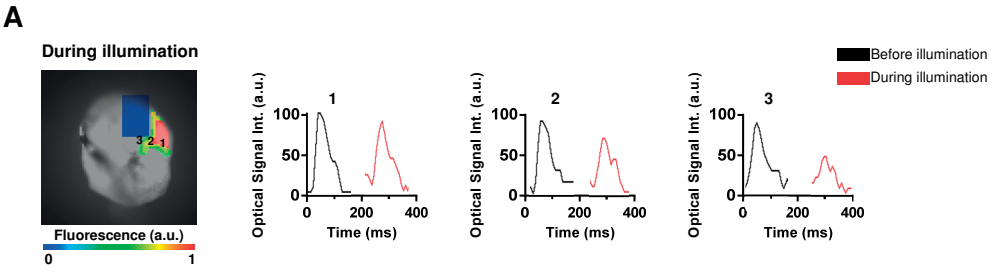

Figure 8. Assessment of depolarization gradient *in vitro*. Optical signal traces from spots 1-3, with 1 being furthest away from the targeted area, before (black) and during (red) illumination (n=8 slices from 6 rats).

curvature (*i.e.*, curvature along the direction of propagation) to transverse curvature (*i.e.*, curvature perpendicular to the direction of propagation) decreased from 0.408 to 0.133 and 0.064 for D, D↑ and D↑↑, respectively (Figure 7F, left). A 12.5- and 25-fold decrease in D (D↓ and D↓↓, respectively), however, resulted in opposite effects, *i.e.* a drop in the percentage of strips showing failure of propagation at the site of partial conduction block (Figure 7C), a decrease in the spatial spread of the depolarization gradients (Figure 7E, D↓ and D↓↓), an increase in r from 0.022 to 0.768 and 0.934 for D, D↓ and D↓↓(Figure 7F, right), and more often continuation of propagation. Taken together, these results indicate that generation of a conduction block that is partially obstructing the pathway of propagation and thereby leaving a narrow isthmus, could indeed result in failure of such propagation through local formation of temporary source-sink mismatches.

DISCUSSION

Anatomical reentry is a key mechanism of potentially lethal heart rhythm disturbances in structural heart disease, and is characterized by AP propagation around a fixed anatomical obstacle. The mechanisms involved in the interruption and therefore termination of anatomical reentry have been mainly ascribed to global temporary modulation of electrophysiological properties through the application of drugs, electrical shocks and/or local permanent modulation of cardiac electrical activity through tissue ablation at critical sites. Here, we investigated optogenetic manipulation of anatomical reentry in cultured ventricular tissue slices. We consider the results as a proof-of-principle demonstration that such arrhythmia could be optogenetically terminated. The mechanism involved in the interruption of the anatomical reentry, as described in our study, is based on the temporary inhibition of excitability in only a specific part of the reentrant pathway via optogenetic modification and patterned illumination technology. As a result, a functional and reversible conduction block is created in this pathway, thereby preventing continuation of reentry and allowing normal activation to resume. Our data regarding optogenetic control of excitability are in line with previous studies. Bruegmann *et al*[9] showed that prolonged illumination of cardiomyocytes expressing wild-type ChR2 resulted in a significant and sustained upward shift in membrane potential. As a result of this light-induced depolarization, the cardiomyocytes can no longer be electrically activated thereby producing a functional conduction block. While light-gated cation channels are mostly used as excitatory tools for optical pacing by generating brief supra-threshold depolarizing stimuli, here we show, by single-cell patch clamping in combination with optical voltage mapping of cardiac tissue slices, that their prolonged activation produces a depolarizing current of sufficient strength and duration to allow inhibition of excitation. In their groundbreaking paper, Arrenberg *et al*[28] were the first to demonstrate that activation of a light-gated chloride pump, resulting in a hyperpolarizing photocurrent, could also inhibit electrical activity in cardiac tissue. In a recent study by Nussinovitch *et al*,[12] a light-gated hyperpolarizing proton pump was used to inhibit electrical activity in cardiomyocytes cultured on multi-electrode array culture dishes. Whether the results of our study depend on the specific use of CatCh, or may be obtained with other

light-gated depolarizing or hyperpolarizing tools as well, remains to be determined. However, certain differences can be expected, especially given the important contribution that the depolarization gradients in the proximity of the illuminated area seem to have in terminating anatomical reentry. While several prior studies reported optogenetic control over cardiac tissue excitability,[9-13] in general, the anti-tachyarrhythmic potential of optogenetics remains relatively poorly studied. In a previous study we investigated the effects of global activation of CatCh on spiral wave tachyarrhythmias in monolayers of atrial cardiomyocytes.[25] The resulting depolarizing photocurrent caused drifting of the spiral waves, leading to critical collision and thereby termination of these waves. In more recent studies, the anti-arrhythmic potential of ChR2(H143R), another depolarizing optogenetic tool, has been explored in whole murine hearts. Here, Bruegmann *et al*[29] and Crocini at al[30] have shown that optogenetic manipulation of ventricular arrhythmias may lead to their termination. They relied on computer simulations to suggest that Na^+ channel inactivation based on ChR2-dependent depolarization may be involved in the underlying anti-arrhythmic mechanism. In the present study, we make use of a controllable *in situ* model of ventricular tachyarrhythmias in which these disturbances are solely based on pre-defined anatomical reentry, thereby allowing more systematic and detailed studies into the underlying anti-arrhythmic mechanisms of optogenetic interventions. Here, patterned illumination was used to generate a transmural conduction block with a width of 600 mm in the pathway of reentry, which resulted in arrhythmia termination in all slices and in all cases. Under these conditions, the reentrant waves were apparently not able to penetrate the illuminated area deep enough via electrotonic conduction to activate the cardiomyocytes at the other side of the functional conduction block and reentry was therefore terminated at once. Of note, such optogenetic termination of an anatomical reentry is based on a fully reversible functional conduction block leaving no tissue damage or electrical dysfunction. Even more interestingly were our experiments in which the conduction block did not fully obstruct the reentrant pathway, but was leaving a narrow isthmus between the two non-illuminated transmural areas of myocardial tissue. Here, the outcome was directly determined by the width of the isthmus, showing more often reentry termination at the site of illumination with further narrowing of the isthmus. From a mechanistic point of view, we showed, through a set of complementary *in silico* and *in situ* studies, extension of a gradient in depolarization from the illuminated area into the isthmus. The *in silico* data revealed that the membrane potential was ranging from -20 mV in the center to -30 mV at the border of the illuminated area and -70 mV in the most distal region (Figure 7D, left frames). In line with these results, the *in situ* data showed a strong reduction (~50%) of the optical signal amplitude in the spot closest to the area of illumination (Figure S5A), thereby indeed suggesting the presence of a graded decrease in excitability. Generation, by patterned illumination, of a transmural conduction block with a width of 600 mm in the pathway of reentry, resulted in arrhythmia termination in all slices and in all cases. Under these conditions, the reentrant waves were apparently not able to penetrate the illuminated area deep enough via electrotonic conduction to activate the cardiomyocytes at the other side of the functional conduction block and reentry was therefore terminated at once. Of note, such optogenetic termination of an anatomical reentry is based on a fully reversible functional

conduction block leaving no tissue damage or electrical dysfunction. Even more interestingly were our experiments in which the conduction block did not fully obstruct the reentrant pathway, but was leaving a narrow isthmus between the two non-illuminated transmural areas of myocardial tissue. Here, the outcome was directly determined by the width of the isthmus, showing more often reentry termination at the site of illumination with further narrowing of the isthmus. This result suggested that local electrical source-sink mismatches resulted in reentry termination, because such mismatches are known to block AP propagation. Earlier work from, among others, Cabo *et al*,[31] Fast *et al*[32] and Rohr *et al*,[27] identified a crucial role for gap junctional coupling in determining these source-sink relationships, with a stronger effect on the load than source for a certain degree of uncoupling. Hence, upon partial uncoupling, electrical signals are able to propagate from a narrow area to a wider area, while initially their propagation stopped at the site of expansion. Our *in silico* study provides novel insight into this matter by showing that enhanced gap junctional conductance increased the spread of depolarization gradients around the illuminated area, thereby expanding the area of effective functional conduction block and reducing the curvature of the entering wavefront. This reduction in curvature was associated with insufficient depolarizing force at the isthmus, giving rise to source-sink mismatch and resulting in propagation failure (Figure 7). This finding is in line with earlier work of Rohr *et al*,[27] which assessed the role of wavefront curvature in AP propagation at suddenly expanding areas of cardiac tissue.

Study limitations and translational considerations

The *in situ* model presented in this study is based on cultured transverse slices of neonatal rat ventricular myocardium and allowed standardized and systematic studies into optogenetic manipulation of anatomical reentry. Slices from the adult rat heart might be more relevant in terms of translation potential, but the requirement of 4 days in culture to allow sufficient CatCh expression together with the fact that cultured cardiac tissue slices from adult rats degenerate much more quickly than those of newborn rats[33, 34] led us to employ neonatal rat hearts. The electrophysiological properties of neonatal rat hearts differ to some extent from those of adult hearts. Neonatal rat hearts, for instance, have weaker Na^+ and repolarizing currents and Cx43 is distributed not only at the intercalated discs but also along the cell borders.[35-38] Hence, the absolute values as reported in our study should be interpreted keeping these differences in mind, although we believe that the overall conclusion remains valid. Furthermore, the model used in our study allowed us to induce a single pre-defined and stable reentrant wave, which was anchored to the left cardiac lumen. In the diseased whole heart, however, these circuits are often fixed to a much more heterogeneous substrate consisting of, for example, highly fibrotic regions with complex shapes and distribution patterns. Because of this structural heterogeneity in diseased hearts, multiple circuits can be maintained and, as a consequence, the identification of the most critical isthmus might be more challenging as its presence could change in time. For this reason, pathologically more relevant and more complex models are needed to assess the translational value of the novel concept of reentry termination "brought to light" in this study.

Another potential hurdle to the clinical translation of our findings might be the current challenge to illuminate a sufficiently large mass of myocardium (*i.e.* beyond the epi- or endocardial surface) in order to produce a photocurrent strong enough for anatomical reentry termination. Although our study shows that full transmural illumination is indeed the most effective way to terminate anatomical reentry, it also reveals that subtransmural illumination could lead to arrhythmia termination. We are, however, aware of the fact that many more studies are needed to assess the therapeutic relevance of our findings, and we therefore consider these data as proof-of-principle for optogenetic termination of anatomical reentry. Such future experiments should include, for example, various gradients and shapes of illumination to better mimic those illumination patterns that can be expected from epi- or endocardial illumination. Indeed, it is known that tissue penetration of 470-nm light is rather poor.[9, 39] Zaglia *et al* confirmed that the intensity of such light applied at the epicardial surface, decreases by 80% when reaching areas of myocardium at a depth of 300 μm.[40] There are, however, several means by which the penetration of light might be improved in order to reach deeper, if this would be needed for effective termination of anatomical reentry in larger hearts, as those of humans. These include the use red-shifted optogenetic tools, such as other ChR2 variants,[41, 42] in combination with, for example, elastic integumentary membranes equipped with multiple μ-LEDs[43] or implantation of injectable hardware-free μ-LEDs inside the myocardium.[44] In addition, more in-depth investigation is needed into the optimal combination of specific light-gated ion channels and illumination protocols with regard to the particular substrate of the arrhythmia, *e.g.* its composition and location. For example, substrates located closer to myocardial surfaces might be more suited for optogenetic targeting than those located deeper in the tissue.

Conclusions

In summary, our data indicate that optogenetic modification of cultured transverse slices of rat myocardial tissue, followed by patterned illumination of a pre-defined area in these slices, allows this area to directly act as a fully reversible functional conduction block shaped by light. Hence, the presence of this block can be tightly controlled in time and space in any desired region of the slice, thereby allowing such a block to be generated in the pathway of anatomical reentry. Depending on the size of the conduction block (*i.e.* the width of the isthmus), reentrant waves are either slowed or halted at the site of illumination. Although our study illustrates that full transmural illumination is the most effective way of anatomical reentry termination, it also shows that this is not absolutely required for termination in our model. This is an important finding, both conceptually (*i.e.* optogenetically induced source-sink mismatches) and practically (*i.e.* no absolute need for full transmural illumination). Computer modeling studies suggest that so-called electrical source-sink mismatches play a crucial role in the mechanism responsible for reentry termination by creating light-induced depolarization gradients that partially obstruct the conduction pathway. The light-guided generation of regional, temporary and reversible conduction block in viable cardiac tissue slices provides a distinctively novel approach to manipulate and terminate anatomical reentry. Thus our data do not only provide novel mechanistic insight into optogenetic control of cardiac electrical function in ventricular

tissue, but that they may also initiate more research into innovative, biology-driven strategies for cardiac arrhythmias therapies.

FUNDING

This work was supported by the Netherlands Organisation for Scientific Research [NWO, Vidi grant 91714336 to D.A.P.]. Additional support was provided by Ammodo [D.A.P. and A.A.F.d.V.] and the Japanese Society of Electrocardiology [Research fellowship 2013 to M.W.].

ACKNOWLEDGMENTS

We thank Cindy Schutte-Bart (Department of Cardiology, LUMC) for assistance with the animal experiments, Stefan Michel (Department of Molecular Cell Biology, LUMC) and Maaike Vreeswijk (Department of Human Genetics, LUMC) for their help in preparing the cardiac tissue slices and Annemarie Kip (Department of Cardiology, LUMC) for LV production.

CONFLICT OF INTEREST

None.

REFERENCES

1. Hsia HH, Marchlinski FE. Electrophysiology studies in patients with dilated cardiomyopathies. Card Electrophysiol Rev. 2002; 6:472-81.
2. Josephson ME, Horowitz LN, Farshidi A, Kastor JA. Recurrent sustained ventricular tachycardia. 1. Mechanisms. Circulation. 1978; 57:431-40.
3. Josephson ME, Almendral JM, Buxton AE, Marchlinski FE. Mechanisms of ventricular tachycardia. Circulation. 1987; 75:III41-7.
4. Connolly SJ, Dorian P, Roberts RS, Gent M, Bailin S, Fain ES, Thorpe K, Champagne J, Talajic M, Coutu B, Gronefeld GC, Hohnloser SH, Optimal Pharmacological Therapy in Cardioverter Defibrillator Patients I. Comparison of beta-blockers, amiodarone plus beta-blockers, or sotalol for prevention of shocks from implantable cardioverter defibrillators: the OPTIC Study: a randomized trial. JAMA. 2006; 295:165-71.
5. Moss AJ, Greenberg H, Case RB, Zareba W, Hall WJ, Brown MW, Daubert JP, McNitt S, Andrews ML, Elkin AD. Long-term clinical course of patients after termination of ventricular tachyarrhythmia by an implanted defibrillator. Circulation. 2004; 110:3760-5.
6. Stevenson WG, Soejima K. Catheter ablation for ventricular tachycardia. Circulation. 2007; 115:2750-60.
7. Ambrosi CM, Klimas A, Yu J, Entcheva E. Cardiac applications of optogenetics. Prog Biophys Mol Biol. 2014; 115:294-304.
8. Entcheva E. Cardiac optogenetics. Am J Physiol Heart Circ Physiol. 2013; 304:H1179-91.
9. Bruegmann T, Malan D, Hesse M, Beiert T, Fuegemann CJ, Fleischmann BK, Sasse P. Optogenetic control of heart muscle in vitro and in vivo. Nat Methods. 2010; 7:897-900.
10. Nussinovitch U, Shinnawi R, Gepstein L. Modulation of cardiac tissue electrophysiological properties with light-sensitive proteins. Cardiovasc Res. 2014; 102:176-87.
11. Nussinovitch U, Gepstein L. Optogenetics for in vivo cardiac pacing and resynchronization therapies. Nat Biotechnol. 2015; 33:750-4.
12. Nussinovitch U, Gepstein L. Optogenetics for suppression of cardiac electrical activity in human and rat cardiomyocyte cultures. Neurophotonics. 2015; 2:031204.
13. Park SA, Lee SR, Tung L, Yue DT. Optical mapping of optogenetically shaped cardiac action potentials. Sci Rep. 2014; 4:6125.
14. Bovetti S, Fellin T. Optical dissection of brain circuits with patterned illumination through the phase modulation of light. J Neurosci Methods. 2015; 241:66-77.
15. Packer AM, Roska B, Hausser M. Targeting neurons and photons for optogenetics. Nat Neurosci. 2013; 16:805-15.
16. Papagiakoumou E. Optical developments for optogenetics. Biol Cell 2013;105 :443-64.
17. Reutsky-Gefen I, Golan L, Farah N, Schejter A, Tsur L, Brosh I, Shoham S. Holographic optogenetic stimulation of patterned neuronal activity for vision restoration. Nat Commun 2013;4:1509.
18. Kleinlogel S, Feldbauer K, Dempski RE, Fotis H, Wood PG, Bamann C, Bamberg E. Ultra light-sensitive and fast neuronal activation with the Ca(2)+-permeable channelrhodopsin CatCh. Nat Neurosci. 2011; 14:513-8.
19. Korhonen T, Hanninen SL, Tavi P. Model of excitation-contraction coupling of rat neonatal ventricular myocytes. Biophys J. 2009; 96:1189-209.
20. Hou L, Deo M, Furspan P, Pandit SV, Mironov S, Auerbach DS, Gong Q, Zhou Z, Berenfeld O, Jalife J. A major role for HERG in determining frequency of reentry in neonatal rat ventricular myocyte monolayer. Circ Res. 2010; 107:1503-11.
21. ten Tusscher KH, Mourad A, Nash MP, Clayton RH, Bradley CP, Paterson DJ, Hren R, Hayward M, Panfilov AV, Taggart P. Organization of ventricular fibrillation in the human heart: experiments and models. Exp Physiol. 2009; 94:553-62.

22. MacCannell KA, Bazzazi H, Chilton L, Shibukawa Y, Clark RB, Giles WR. A mathematical model of electrotonic interactions between ventricular myocytes and fibroblasts. Biophys J. 2007; 92:4121-32.

23. Williams JC, Xu J, Lu Z, Klimas A, Chen X, Ambrosi CM, Cohen IS, Entcheva E. Computational optogenetics: empirically-derived voltage- and light-sensitive channelrhodopsin-2 model. PLoS Comput Biol. 2013; 9:e1003220.

24. Boyle PM, Williams JC, Ambrosi CM, Entcheva E, Trayanova NA. A comprehensive multiscale framework for simulating optogenetics in the heart. Nat Commun. 2013; 4:2370.

25. Bingen BO, Engels MC, Schalij MJ, Jangsangthong W, Neshati Z, Feola I, Ypey DL, Askar SF, Panfilov AV, Pijnappels DA, de Vries AA. Light-induced termination of spiral wave arrhythmias by optogenetic engineering of atrial cardiomyocytes. Cardiovasc Res. 2014; 104:194-205.

26. Kleber AG, Rudy Y. Basic mechanisms of cardiac impulse propagation and associated arrhythmias. Physiol Rev. 2004; 84:431-88.

27. Rohr S, Kucera JP, Fast VG, Kleber AG. Paradoxical improvement of impulse conduction in cardiac tissue by partial cellular uncoupling. Science. 1997; 275:841-4.

28. Arrenberg AB, Stainier DY, Baier H, Huisken J. Optogenetic control of cardiac function. Science. 2010; 330:971-4.

29. Bruegmann T, Boyle PM, Vogt CC et al Optogenetic defibrillation terminates ventricular arrhythmia in mouse hearts and human simulations. J Clin Invest 2016; 126:3894-904.

30. Crocini C, Ferrantini C, Coppini R et al Optogenetics design of mechanistically-based stimulation patterns for cardiac defibrillation. Sci Rep. 2016; 6:35628.

31. Cabo C, Pertsov AM, Baxter WT, Davidenko JM, Gray RA, Jalife J. Wave-front curvature as a cause of slow conduction and block in isolated cardiac muscle. Circ Res. 1994; 75:1014-28.

32. Fast VG, Kleber AG. Block of impulse propagation at an abrupt tissue expansion: evaluation of the critical strand diameter in 2- and 3-dimensional computer models. Cardiovasc Res. 1995; 30:449-59.

33. Obreztchikova MN, Sosunov EA, Plotnikov A, Anyukhovsky EP, Gainullin RZ, Danilo P, Yeom ZH, Robinson RB and Rosen MR. Developmental changes in IKr and IKs contribute to age-related expression of dofetilide effects on repolarization and proarrhythmia. Cardiovascular research. 2003; 59:339-50.

34. Antzelevitch C. Are M cells present in the ventricular myocardium of the pig? A question of maturity. Cardiovascular research. 1997; 36:127-8.

35. Cordeiro JM, Panama BK, Goodrow R, Zygmunt AC, White C, Treat JA, Zeina T, Nesterenko VV, Di Diego JM, Burashnikov A and Antzelevitch C. Developmental changes in expression and biophysics of ion channels in the canine ventricle. Journal of molecular and cellular cardiology. 2013; 64:79-89.

36. Kaneko M, Coppen SR, Fukushima S, Yacoub MH and Suzuki K. Histological Validation of Heart Slices as a Model in Cardiac Research. Journal of Cell Science & Therapy. 2012; 3:4.

37. van Kempen MJ, Fromaget C, Gros D, Moorman AF, Lamers WH. Spatial distribution of connexin43, the major cardiac gap junction protein, in the developing and adult rat heart. Circ Res. 1991; 68:1638-51.

38. Popa MA and Corotchi MC. An in vitro method for adhesion of fresh adult murine heart slices on Collagen-coated surfaces. Annals of the Romanian Society for Cell Biology. 2015; 20:4.

39. Vogt CC, Bruegmann T, Malan D, Ottersbach A, Roell W, Fleischmann BK and Sasse P. Systemic gene transfer enables optogenetic pacing of mouse hearts. Cardiovasc Res 2015 May 1; 106:338-43.

40. Zaglia T, Pianca N, Borile G, Da Broi F, Richter C, Campione M, Lehnart SE, Luther S, Corrado D, Miquerol L and Mongillo M. Optogenetic determination of the myocardial requirements for extrasystoles by cell type-specific targeting of ChannelRhodopsin-2. Proceedings of

the National Academy of Sciences of the United States of America. 2015; 112:E4495-504.

41. Lin JY, Knutsen PM, Muller A, Kleinfeld D and Tsien RY. ReaChR: a red-shifted variant of channelrhodopsin enables deep transcranial optogenetic excitation. Nature neuroscience. 2013; 16:1499-508.

42. Prigge M, Schneider F, Tsunoda SP, Shilyansky C, Wietek J, Deisseroth K and Hegemann P. Color-tuned channelrhodopsins for multiwavelength optogenetics. The Journal of biological chemistry. 2012; 287:31804-12.

43. Xu L, Gutbrod SR, Bonifas AP, Su Y, Sulkin MS, Lu N, Chung HJ, Jang KI, Liu Z, Ying M, Lu C, Webb RC, Kim JS, Laughner JI, Cheng H, Liu Y, Ameen A, Jeong JW, Kim GT, Huang Y, Efimov IR and Rogers JA. 3D multifunctional integumentary membranes for spatiotemporal cardiac measurements and stimulation across the entire epicardium. Nature communications. 2014; 5:3329.

44. Kim TI, McCall JG, Jung YH, Huang X, Siuda ER, Li Y, Song J, Song YM, Pao HA, Kim RH, Lu C, Lee SD, Song IS, Shin G, Al-Hasani R, Kim S, Tan MP, Huang Y, Omenetto FG, Rogers JA and Bruchas MR. Injectable, cellular-scale optoelectronics with applications for wireless optogenetics. Science. 2013; 340:211-6.

SUPPLEMENTAL MATERIAL

Detailed Methods

Preparation of transverse rat ventricular tissue slices

All animal experiments were approved by the Animal Experiments Committee of Leiden University Medical Center (LUMC) and done in accordance with the Guide for Care and Use of Laboratory Animals as stated by the US National Institutes of Health. Transverse ventricular tissue slices were obtained from neonatal Wistar rats. The 2-day-old rats were anaesthetized by 4-5% isoflurane inhalation and adequate anesthesia was confirmed by the absence of reflexes. After the chest was opened and the inferior vena cava was cut off with scissors, the right atrium was punctured with a 19 gauge needle. The heart was perfused through this needle with pre-warmed and oxygenated phosphate-buffered saline (PBS) containing 10 IU/ml heparin to replace the blood. Subsequently, the heart was excised and stored in ice-cold and pre-oxygenized modified Tyrode's solution (MTS; NaCl 143 mmol/l, KCl 5.4 mmol/l, NaH_2PO_4 0.3 mmol/l, $MgCl_2$ 0.5 mmol/l, HEPES 5 mmol/l, $CaCl_2$ 0.9 mmol/l, glucose 5.5 mmol/l, 2,3-butanedione monoxime 20 mmol/l). Before slicing, the heart was embedded in 4% low melting point agarose (type VII-A; Sigma-Aldrich, St. Louis, MO) dissolved in MTS at 37°C and subsequently fixed to the sample holder of the vibratome (VT1200S, Leica Microsystems, Rijswijk, the Netherlands) using cyanoacrylate-based super glue.[1] The sample was then quickly covered with ice-cold and pre-oxygenated MTS and cut into 150-µm thick tissue slices using Derby extra super stainless double edge razor blades. Each slice was placed onto the semi-porous membrane (0.4 µm pore size) of a PICM0RG50 cell culture insert (Millipore, Amsterdam-Zuidoost, the Netherlands) in a 35-mm diameter Petri dish containing sterilized MTS of room temperature (RT) and gradually warmed to 37°C (Figure S1A and S1B). Next, the MTS was replaced with pre-warmed culture medium Dulbecco's modified Eagle's medium (DMEM; Life Technologies Europe, Bleiswijk, the Netherlands) supplemented with 1% heat-inactivated fetal bovine serum (HI-FBS; Life Technologies Europe), 1× penicillin-streptomycin (Life Technologies Europe), 1× B-27 supplement (Life Technologies Europe) and 5 µM Z-Asp-2,6- dichlorobenzoyloxymethylketone (Santa Cruz Biotechnology, Heidelberg, Germany) and the slice was kept at 37°C in humidified 95% air-5% CO_2 (culture conditions).

Lentiviral gene transfer

The construction of the lentiviral vector shuttle plasmids pLV.MHCK7.CatCh~eYFP.WHVPRE and pLV.MHCK7.eYFP.WHVPRE and the production of the corresponding viral vectors designated LV.CatCh~eYFP↑ and LV.eYFP↑, respectively, have been described previously.[2] The cardiac tissue slices were placed on a semi-porous membrane and genetically modified at the same day. A concentrated viral vector suspension was added directly on top of the slices with an inoculum consisting of 1 µl of culture medium containing 10 µg/ml diethylaminoethyl-dextran (Carl Roth, Karlsruhe, Germany) and 9 µl of LV suspension. After 30 minutes, the semi-porous membrane was transferred to a culture dish filled with 1 ml medium containing 90 µl LV suspension and diethylaminoethyl-dextran at a final concentration of 1 µg/ml. After 24 h at

37°C in humidified 95% air-5% CO_2, the tissue was washed twice with fresh culture medium and then kept under culture conditions for 4 additional days.

Patch clamp

As reported previously,[3] patch clamp recordings were performed under an inverted microscope Zeiss Axiovert 35 (Carl Zeiss AG, Oberkochen, Germany) at 20-23°C using perforated patch clamp technique and a conventional patch clamp equipment consisting of a MultiClamp 700B amplifier and a Digidata 1440A A/D converter (Molecular Devices, Sunnyvale, CA, USA), all connected to a personal computer and driven by commercially available MultiClamp 700B Commander and Clampex v10.3 software (Molecular Devices). Throughout experiments, the current and voltage outputs of amplifier were continuously sampled at intervals of 100 μs and recorded onto personal computer after low-pass filtered at 2-4 kHz with a four-pole Bessel filter. Neonatal rat ventricular cardiomyocytes (NRVCs) were isolated from hearts of 2-day-old Wistar rat pups using collagenase type I (450 U/ml; Worthington, Lakewood, NJ) and DNase I (1,8 U/ml in solution A; Sigma-Aldrich) solution in a shaking water bath at 37°C for 2 × 35 minutes, as described previously.[3] Isolated cells were plated on round glass coverslips (15-mm diameter, Thermo Fisher Scientific Gerhard Menzel B.V. & Co. KG, Braunschweig, Germany) coated with fibronectin (Sigma-Aldrich) in 24-well plates (Corning Life Sciences, Amsterdam, the Netherlands) at the density of 15×10^3 cells/well. Directly after isolation, NRVCs were transduced with LV.CatCh~eYFP↑ by adding the lentiviral vector suspension into the cell suspension. To prevent proliferation of non-cardiomyocytes, 16 hours after platting, cultures were treated for 2 hours with mitomycin-C (10 μg/mL; Sigma-Aldrich). NRVCs expressing CatCh (CatCh-NRVCs) were kept in a humidified incubator at 37 °C and 5% CO_2 and refreshed daily with culture medium consisting of a 1:1 mixture of DMEM (Life Technologies Europe) and Ham's F10 supplemented with 5% HS, penicillin (100 U/ml, Life Technologies) and streptomycin (100 μg/ml, Life Technologies). CatCh-NRVCs were transferred from culture medium to an external cellular solution containing (in mM): 126 NaCl, 11 glucose, 10 HEPES, 5.4 KCl, 1 $MgCl_2$, and 1.8 $CaCl_2$ (adjusted to pH 7.40 with NaOH). Approximately within 15-60 minutes after superfusion of external cellular solution, patch clamp experiments were conducted. For CatCh-NRVCs, only solitary cells expressing eYFP were selected for the experiments. The pipettes were fabricated from borosilicate glass capillaries (1.5 mm outer diameter and 1.17 mm inner diameter, Harvard Apparatus, Kent, UK) with a vertical puller (P-30, Sutter Instruments, Novato, CA, USA). CPM-2 coating and polishing mircroforege (ALA Scientific Instruments, Farmingdale, NY, USA) was employed for fire-polishing to reshape and smooth pipette tips. Pipettes had typical electrical resistances of 2-3 MW in the external cellular solution when filled with the internal solution. Here, an ATP-, GTP and EGTA-free pipette solution containing (in mM): 80 potassium DL-aspartate, 40 KCl, 8 NaCl, 5.5 glucose, 5 HEPES, and 1 $MgCl_2$ (adjusted to pH 7.20 with KOH) was used to tip-fill patch pipettes, and the same pipette solution containing nystatin (120-200 μg/ml; Sigma-Aldrich) was used to back-fill the pipettes. The giga-ohm seal was formed by continuously applied 10-ms voltage steps from 0 to +5 mV at 10 Hz. After reaching giga-ohm seal, the holding potential was set to -50 mV. The series resistance

was monitored and shown progressively decline. Recordings were started after the series resistance had reached steady state of 15-10 MΩ stable (*i.e.* after 20-30 min). The integrity of the perforated patch was checked during and after recording for every experiments. We noted that the rupture of patch membrane abruptly increased capacitive current, unleashed the pipette solution to diffuse into the cells and caused an irreversible contracture because a specific chelator for calcium EGTA was absence. Therefore, we discarded those cells that showed sudden appearance of the capacitive current or the irreversible contracture under the microscope to ensure reliability of recordings. Cell capacitance (C_m) was calculated from capacitive transient currents evoked during 5 mV steps from a holding potential of -50 mV and electrically removed with amplifier. To minimize voltage error and fetch the adequacy of the voltage-clamp, pipette series resistance was routinely monitored and electrically compensated by >75%. The estimated liquid-junction potential of 11 mV were corrected.

To investigate light induced voltage shift and photo current, we integrated the inverted microscope Zeiss Axiovert 35 (Carl Zeiss AG) with a blue light illumination device M470L3 collimated light-emitting diode (LED) light sources for microscopy driven by the T-Cube LED driver (Thorlabs GmbH, Munich, Germany). The LED based illumination system was controlled by STG4002 2-channels stimulus generator and MC_Stimulus program (Multi Channel Systems MCS GmbH, Reutlingen, Germany) to generate light pluses with various light intensities and durations. A precise 500-ms light pulse at various intensities was employed to determine the minimum light intensity needed for action potential generation with a stable voltage shift. The minimum light intensity (0.65 mW/mm^2) at which light stimulus induced action potential with a stable voltage shift was taken as the threshold for investigating prolonged light stimulation induced action potentials, followed by prolonged depolarization. Subsequently, the same minimum light intensity was also used to characterize photo current in CatCh-NRVCs. At holding potential of -40 mV, peak currents (I_{pk}), steady-state current (I_{ss}), desensitization time constant (t_{des}) and channel closing time constant (t_{off}) were determined from photo current recordings during 500-ms light pulse.

Immunohistology

At day 5 of culture, slices were fixed with 4% buffered formaldehyde (Added Pharma, Oss, the Netherlands) for 30 minutes at RT, washed three times with PBS and permeabilized by incubation for 15 minutes at RT with 0.1% Triton-X100 in PBS. Next, slices were incubated overnight at 4°C with antibodies directed against sarcomeric α-actinin (mouse IgG1; Sigma-Aldrich, A7811), Col1 (rabbit IgG; Abcam, Cambridge, MA, ab292), Cx43 (rabbit Ig; Sigma-Aldrich, C6219) or active caspase-3 (rabbit IgG; Abcam, ab2303). All primary antibodies were diluted 1:200 in PBS + 1% FBS (Life Technologies Europe). The day after, slices were washed three times with PBS, incubated for 4 hours at 4°C with the corresponding Alexa Fluor 568-conjugated secondary antibodies (Life Technologies Europe; 1:400 dilution in PBS + 5% FBS) and again washed three times with PBS. For staining of mitochondria, slices were incubated with MitoTracker Red CMXRos (Life Technologies Europe) at a concentration of 200 nM for 30 minutes at 37°C. Subsequently, slices were fixed with 4% buffered formaldehyde and

washed three times with PBS. Nuclear staining was performed at RT with 10 mg/ml Hoechst 33342 (Life Technologies Europe) in PBS and followed by a single wash with PBS. Finally, slices were mounted in Vectashield mounting medium (Vector Laboratories, Burlingame, CA) on top of glass slides. Images were acquired with a confocal laser scanning microscope (LSM 710; Zeiss Nederland, Sliedrecht, the Netherlands). For quantification of CatCh+ cells, images were taken at 63× magnification from 7 different areas in the CatCh↑ slice (n=3 slices, 3 rats) using the confocal microscope Leica TCS SP8 X WLL (Leica Microsystems, Rijswijk, the Netherlands).

Integrated system for optical mapping and patterned illumination

The optical mapping system was engineered to allow recording of electrical activation with the voltage-sensitive dye di-4-ANEPPS (Life Technologies Europe) and patterned illumination with blue light (470 nm) (Figure S1C). To this end, a patterned illumination device, the Polygon400 (Mightex Systems, Toronto, ON) was connected through a cube containing a blue light-specific dichroic mirror (reflect 350-500 nm; pass >513 nm, FF506-Di03-25x36, Semrock, Rochester, NY) to the cube for di-4-ANEPPS and the MiCAM ULTIMA-L imaging system (SciMedia, Costa Mesa, CA). The cube for di-4-ANEPPS contained an excitation filter (pass 525±25 nm, FF03-525/50-25, Semrock), a dichroic mirror (reflect 520-560 nm; pass >600 nm, custom made, SciMedia) and an emission filter (pass >590 nm, custom made, SciMedia). For optical mapping with Di-4-ANBDQBS (52.5 μM final concentration), the cube contained an excitation filter (pass 650±27 nm, FF01-650/54-27, Semrock), a dichroic mirror (reflect 350-676 nm; pass 695-950 nm, FF685-Di02-25 × 35, Semrock) and an emission filter (pass >715 nm, FF01-715/LP-25, Semrock).The Polygon400 is a device based on digital micromirrors that in combination with the custom-made software Polylite (Mightex Systems), allows projection of any shape directly onto the living sample. The light from a high-power LED source (470 nm, 50 W, type-H, Mightex Systems) is guided through a liquid light guide to the Polygon400, reflected by the dichroic mirror and finally projected onto the sample through a 5× objective lens (Leica Microsystems, Wetzlar, Germany). Using this particular setup, it was possible to illuminate a maximal area of 1.78 × 3.1 mm with a pixel resolution of 3.6 μm.

Optical mapping

Optical voltage mapping was employed to assess the functional consequences of CatCh-generated photocurrents in transverse ventricular tissue slices kept for 5 days under culture conditions. Electrical activity was visualized using the voltage-sensitive dye di-4-ANEPPS. On day 5 of culture, slices were incubated for 30 min at 37°C with pre-oxygenized MTS containing 1.8 instead of 0.9 mmol/l $CaCl_2$ (MTS+) and 12.5 mmol/l di-4-ANEPPS . Next, slices were washed with pre-oxygenized MTS+ of 37°C and transferred to another cell culture insert in a Petri dish with warm MTS+. Subsequently, optical mapping was performed at 37°C. To prevent drying of the slice surface, no more than 2 slices were placed on the same inserts and mapping experiments typically did not exceed 30 min. Optical voltage signals were analyzed using BrainVision Analyzer 1103 software (Brainvision, Tokyo, Japan). As measure of APD the period

between the time point of maximal upstroke velocity and 80% repolarization (APD_{80}) was taken. Slices were stimulated either electrically with an epoxy-coated unipolar platinum electrode (FHC, Bowdoin, ME) using 2-ms rectangular pulses of 1.5 V or optically with 10-ms 470-nm light pulses, coming from the Polygon400, at the maximum input voltage tolerated by the system (irradiance 0.68 mW/mm^2). A specialized stimulus generator (STG 2004) with corresponding software (MC Stimulus II; both from Multichannel Systems, Reutlingen, Germany) was used to perform both electrical and optical stimulation. Reentry was induced by electrical pacing using a 9-beat driving train with a basic CL of 100-150 ms and a single extrastimulus of 20-80 ms. After confirmation of the presence of reentrant conduction, slices were exposed to 470-nm LED light for 500 ms using the patterned illumination device at 0.68 mW/mm^2. For baseline shift adjustment during illumination, several filters were applied, which allowed interpretation of signals 30 ms after initiation of local light exposure.

Numerical Methods

The neonatal rat ventricular cardiomyocytes were modeled according to the formulation of Korhonen *et al*,[4] with adaptations by Hou *et al*.[5] The complex intracellular Ca^{2+} diffusion between the sarcolemma and the perinuclear sarcoplasmic reticulum was replaced by a simple Ca^{2+}-handling process adopted from tenTusscher *et al*.[6] Cardiac myofibroblasts were modeled according to the passive formulation of MacCannell *et al*,[7] whereas the empirically derived model of ChR2 (current-enhanced mutant H134R) by Williams *et al*[8] was used together with the parameter set established by Boyle *et al*[9] to implement optogenetics. Eight confluent monolayer stripes (12.75 × 2.8 mm) were constructed as arrays of 1145 cell sites with 17% myofibroblasts. Each site was occupied by either a cardiomyocyte or a myofibroblast. The cardiomyocytes in the model coupled electrically to each other via an intercellular coupling coefficient D=0.001±0.0002 cm^2/ms, which describes the passive diffusion of transmembrane voltage between cells and therefore biophysically correlates with gap junctional conductance.[10] For consistency with *in vitro* experiments, cardiomyocytes exhibiting different electrophysiological properties were modeled using a random number generator to create spatial distributions of probabilities for each ionic current/flux produced by a cardiomyocyte. These probabilities were then used to modulate the maximal channel conductance such that the peak value of the associated current/flux ranged from 50 to 150% of the mean value. The myofibroblasts in the stripes coupled electrically to the cardiomyocytes through a gap junctional coupling coefficient Ggap of 0.5 nS/pF.[11] The temporal part of the mathematical equation for the transmembrane potential in the two-dimensional stripe model with ChR2-expressing cardiomyocytes and 17% myofibroblasts was solved using the forward Euler method with a time step δt=0.005 ms. The spatial part was solved using a centered finite differencing scheme and space step $\delta x=\delta y$=0.00625 cm on a 5-point stencil.Each stripe was electrically paced from one side, at a CL of 500 ms, with a 2-ms current stimulus of 100 pA (Figure 7A). Wave propagation was then studied in the stripes in the presence of virtual irradiation over a rectangular area 600 × 25% or 75% of the transmural width (2.8 mm; Figure 7A).

Supplementary Figures

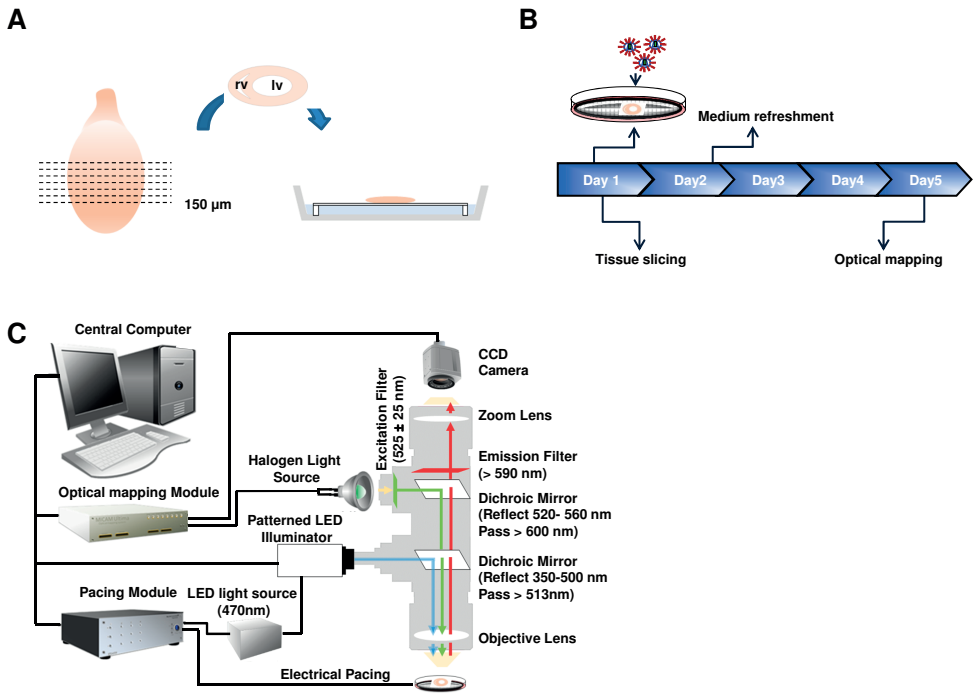

Supplementary Figure 1. Experimental design. A, Transverse ventricular tissue slice preparation. Hearts from 2-day-old neonatal rats were excised and, after flushing out the blood, transverse slices were prepared. Subsequently, the slices were placed onto semi-porous cell culture inserts and maintained for 4 days under culture conditions. B, Experimental timeline. Slices were transduced with LV.eYFP↑ or LV.CatCh~eYFP↑ on the day of preparation, while on day 5 of culture, optical mapping or histological analysis was performed. C, Setup of the system used for optical voltage mapping and patterned LED illumination.

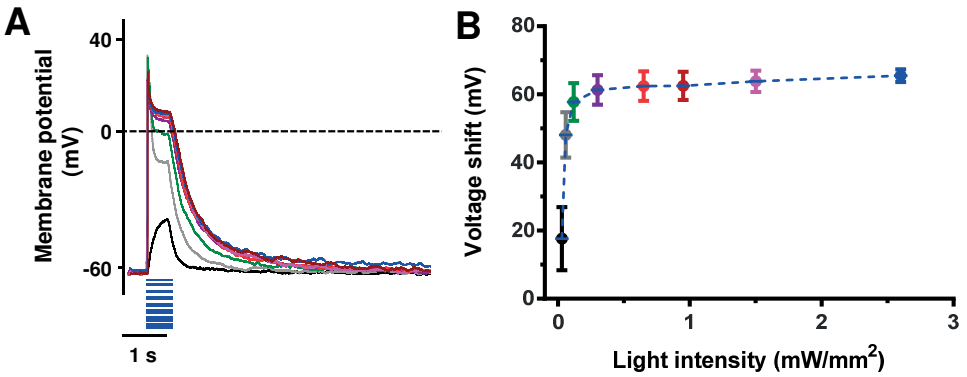

Supplementary Figure 2. Characterization of CatCh light-intensity dependence. B-C, Effect on membrane potential of exposing CatCh-NRVCs to 500-ms blue (470 nm) light pulse of different intensity (n=5).

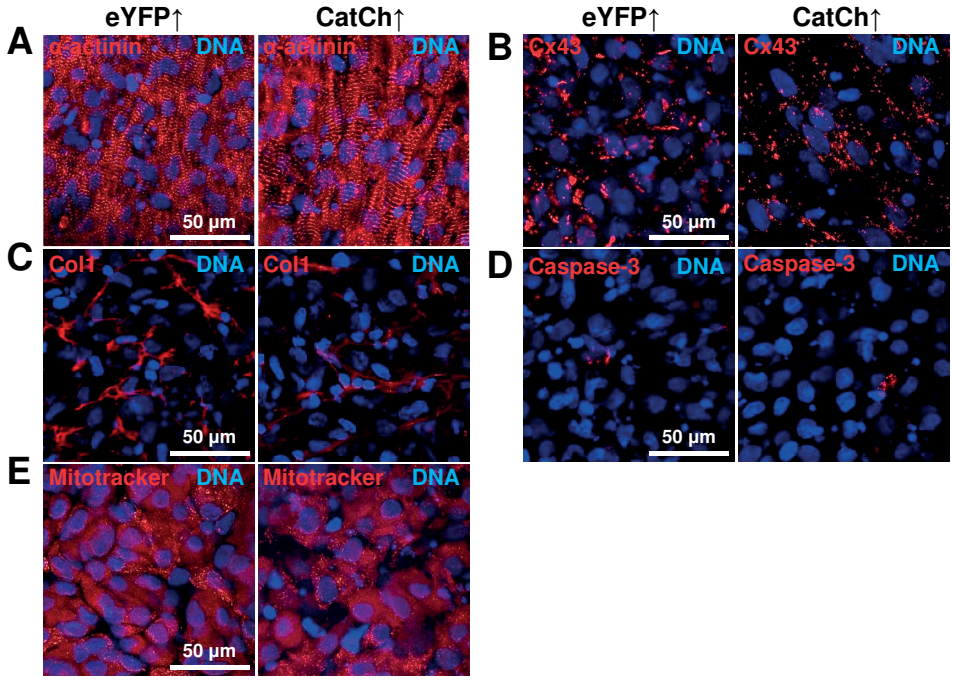

Supplementary Figure 3. (Immuno)histological staining of cultured ventricular slices. The slices were transduced 4 days earlier with LV.eYFP↑ (left) or LV.CatCh~eYFP↑ (right) for nuclei (DNA; blue) and α-actinin (A), Cx43 (B), Col1 (C), caspase-3 (D) or Mitotracker (E), all labeled in red (n=3 for both eYFP↑ and CatCh↑ slices).

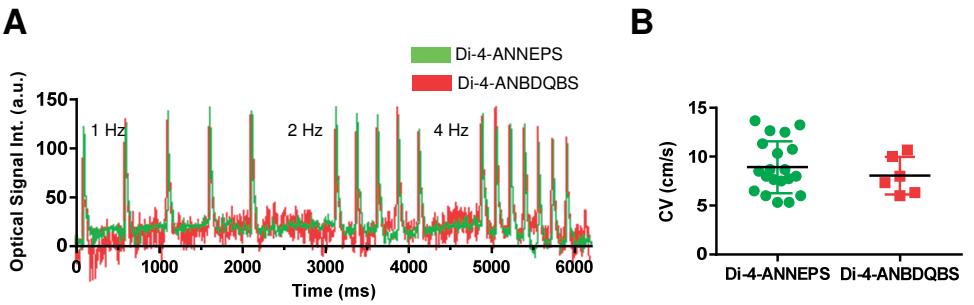

Supplementary Figure 4. Comparison of optical voltage mapping data of electrically stimulated CatCh↑ slices that were loaded with Di-4-ANEPPS or Di-4-ANBDQBS. A, Representative optical traces recorded during electrical stimulation at 1, 2, and 4 Hz. B, CVs measured during 1-Hz electrical stimulation showing no significant difference between slices loaded with Di-4-ANEPPS and those loaded with Di-4-ANBDQBS as determined by the unpaired t-test (nDi-4-ANEPPS=20 slices from 9 rats and nDi-4-ANBDQBS=6 slices from 6 rats).

Supplementary References

1. Brandenburger M, Wenzel J, Bogdan R, Richardt D, Nguemo F, Reppel M, Hescheler J, Terlau H, Dendorfer A. Organotypic slice culture from human adult ventricular myocardium. Cardiovasc Res. 2012; 93:50-9.
2. Bingen BO, Engels MC, Schalij MJ, Jangsangthong W, Neshati Z, Feola I, Ypey DL, Askar SF, Panfilov AV, Pijnappels DA, de Vries AA. Light-induced termination of spiral wave arrhythmias by optogenetic engineering of atrial cardiomyocytes. Cardiovasc Res. 2014; 104:194-205.
3. Engels MC, Askar SF, Jangsangthong W, Bingen BO, Feola I, Liu J, Majumder R, Versteegh MI, Braun J, Klautz RJ, Ypey DL, De Vries AA, Pijnappels DA. Forced fusion of human ventricular scar cells with cardiomyocytes suppresses arrhythmogenicity in a co-culture model. Cardiovasc Res. 2015; 107:601-12.
4. Korhonen T, Hanninen SL, Tavi P. Model of excitation-contraction coupling of rat neonatal ventricular myocytes. Biophys J. 2009; 96:1189-209.
5. Hou L, Deo M, Furspan P, Pandit SV, Mironov S, Auerbach DS, Gong Q, Zhou Z, Berenfeld O, Jalife J. A major role for HERG in determining frequency of reentry in neonatal rat ventricular myocyte monolayer. Circ Res 2010;107:1503-11.
6. ten Tusscher KH, Mourad A, Nash MP, Clayton RH, Bradley CP, Paterson DJ, Hren R, Hayward M, Panfilov AV, Taggart P. Organization of ventricular fibrillation in the human heart: experiments and models. Exp Physiol. 2009; 94:553-62.
7. MacCannell KA, Bazzazi H, Chilton L, Shibukawa Y, Clark RB, Giles WR. A mathematical model of electrotonic interactions between ventricular myocytes and fibroblasts. Biophys J. 2007; 92:4121-32.
8. Williams JC, Xu J, Lu Z, Klimas A, Chen X, Ambrosi CM, Cohen IS, Entcheva E. Computational optogenetics: empirically-derived voltage- and light-sensitive channelrhodopsin-2 model. PLoS Comput Biol. 2013; 9:e1003220.
9. Boyle PM, Williams JC, Ambrosi CM, Entcheva E, Trayanova NA. A comprehensive multiscale framework for simulating optogenetics in the heart. Nat Commun. 2013; 4:2370.
10. Clayton RH, Bernus O, Cherry EM, Dierckx H, Fenton FH, Mirabella L, Panfilov AV, Sachse FB, Seemann G, Zhang H. Models of cardiac tissue electrophysiology: progress, challenges and open questions. Prog Biophys Mol Biol. 2011; 104:22-48.
11. Henriquez AP, Vogel R, Muller-Borer BJ, Henriquez CS, Weingart R, Cascio WE. Influence of dynamic gap junction resistance on impulse propagation in ventricular myocardium: a computer simulation study. Biophys J. 2001; 81:2112-21.